Variable altitude cognizant Slepian functions

Alain M. Plattner[1*], Erwan Mazarico[2] and Christian Gerhards[3]

[1*]Department of Geological Sciences, University of Alabama, Tuscaloosa, AL, USA.
[2]NASA Goddard Space Flight Center, Greenbelt, MD, USA.
[3]Institute of Geophysics and Geoinformatics, TU Bergakademie Freiberg, Freiberg, SN, Germany.

*Corresponding author(s). E-mail(s): amplattner@ua.edu;
Contributing authors: erwan.m.mazarico@nasa.gov;
christian.gerhards@geophysik.tu-freiberg.de;

Abstract

We present an approach to calculate potential fields on a planet's surface from regionally confined gradient data at spacecraft altitude, such as measurements of magnetic fields or gravitational acceleration. Our method uses altitude cognizant Slepian functions with a reference radial position that varies as a function of longitude and latitude. This is an evolution from previous altitude cognizant Slepian functions which use a fixed reference radial position. We demonstrate the advantage of these variable altitude cognizant Slepian functions over the fixed altitude cognizant Slepian functions and the classical Slepian functions using numerical tests.

Keywords: spherical harmonics, geodesy, geomagnetism, planetary science

1 Introduction

Spherical harmonics are a popular basis of functions for describing magnetic or gravity fields of planetary bodies (e.g., Olsen et al, 2007; Finlay et al, 2020; Alken et al, 2021; Morschhauser et al, 2014; Langlais et al, 2019; Purucker and Nicholas, 2010; Tsunakawa et al, 2015; Plattner et al, 2023; Jekeli, 2007; Lemoine et al, 2013; Goossens et al, 2019; Genova et al, 2016, 2019). The properties of spherical harmonics allow for an easy separation of spatial wavelengths as well as simple re-evaluation of a potential or its spatial derivative at any altitude above the planet's surface. A disadvantage of spherical harmonics is that each basis function has a global footprint, meaning that their near-zero values cover only a small fraction of the sphere. This renders it difficult to solve for regional solutions from regional data without regularization. However, local solutions may be desirable or even necessary when variable data quality would regionally allow for higher resolution potential field models, or when data are only regionally available.

Several methods have been developed to solve for regional potential fields from regional data including equivalent source dipoles (ESD, e.g., Toyoshima et al, 2008; Oliveira et al, 2015; Hood, 2015, 2016), regional mascons (e.g., Lemoine et al, 2007; Rowlands et al, 2010; Wittick and Russell, 2019), revised spherical cap harmonic analysis (R-SCHA, e.g., Thébault et al, 2006a,b), spherical wavelets (e.g., Freeden and Windheuser, 1997; Michel, 2002; Holschneider et al, 2003; Chambodut et al, 2005; Panet et al, 2006; Freeden and Schreiner, 2006; Mayer and Maier, 2006; Freeden and Gerhards, 2010; Gerhards, 2012, 2014), and altitude cognizant Slepian functions (Plattner and Simons, 2017; Plattner and Johnson, 2021, 2023). Of these methods, the altitude cognizant Slepian functions are a special case because they are not truly local. Instead, they are constructed as linear combinations of spherical harmonics in an optimization problem. This optimization problem minimizes energy outside of the target region and optimizes the conditioning under reevaluation from spacecraft altitude to the planet's surface. As a consequence, the local solutions using altitude cognizant Slepian functions are regionally representative linear combinations of spherical harmonics with a finite maximum spherical harmonic degree. They have all the benefits of spherical harmonics but represent the potential field only locally.

Altitude cognizant Slepian functions evolved from the classical scalar valued Slepian functions of Albertella and Sacerdote (2001); Wieczorek and Simons (2005); Simons et al (2006) and Simons and Dahlen (2006), and the classical vector valued Slepian functions of Maniar and Mitra (2005); Mitra and Maniar (2005); Jahn and Bokor (2012) and Plattner and Simons (2014). Spatiospectral concentration of one-dimensional functions was originally presented by Slepian and Pollak (1961) and Landau and Pollak (1961). The efficient numerical construction of Slepian functions was greatly aided by the expressions for integrals of Eshagh (2009), as well as the commuting operators of Grünbaum et al (1982); Jahn and Bokor (2014) and Michel et al (2022). These improvements mostly benefited the construction of Slepian functions for spherical caps. Bates et al (2017) presented an efficient way to approximate Slepian functions for general regions based on spherical cap Slepian functions.

Attempts to use classical Slepian functions for calculating a potential field on a planet's surface from data collected at spacecraft altitude indicated suboptimal performance (Plattner and Simons, 2015b). This may be a consequence of the construction of classical Slepian functions which emphasize the higher spherical harmonic degrees to maximize spatial concentration. As a consequence, a local basis consisting of the best-concentrated classical Slepian functions is biased towards the higher spherical harmonic degrees of the chosen bandwidth. When solving for a potential field on a planet's surface from data at spacecraft altitude, high spherical harmonic degrees are disproportionately amplified, leading to poor conditioning of the problem. Altitude cognizant Slepian functions aim to overcome this issue by including the degree-dependent amplification into the optimization problem of the construction of the Slepian functions (Plattner and Simons, 2017). Michel and Simons (2017) address the generalized inverse problem for regional data using Slepian functions.

Altitude cognizant Slepian functions have been used for calculating magnetic field models on the surface of planets from regional data. Plattner and Simons (2015a) image the crustal magnetic field of Mars' South Pole, the region for which the highest-quality data (lowest altitude, nighttime) from the Mars Global Surveyor spacecraft were available. Plattner and Johnson (2021) study a non-axisymmetric signal in Mercury's core magnetic field. Plattner and Johnson (2023) present a generalized approach to calculate regional power spectra from regional data using altitude cognizant Slepian functions for the construction of regional models.

The altitude cognizant Slepian functions of Plattner and Simons (2017, 2015a); Plattner and Johnson (2021), and Plattner and Johnson (2023) are constructed for a single reference spacecraft radial position r_s. This does not preclude using this method for data with variable radial position, but the performance of the altitude cognizant Slepian functions degrades with increasing difference between the data radial positions and r_s. In this paper, we present altitude cognizant Slepian functions for radial positions that are a function of longitude and latitude. We demonstrate using numerical tests that these variable altitude cognizant Slepian functions have the potential to substantially reduce the error in the potential field compared to the fixed altitude cognizant Slepian functions of Plattner and Simons (2017) when the spacecraft data radial positions show a strong dependence on the latitude, longitude, or both. Several past and present spacecraft have elliptical orbits, including MESSENGER (Solomon et al, 2007), MAVEN (Jakosky et al, 2015) and BepiColombo (Benkhoff et al, 2010; Kasaba et al, 2020). Analysis of these spacecrafts' data as well as data from flybys may benefit from the variable altitude cognizant Slepian functions presented in this paper.

2 Prerequisites

We use the following notations. Scalar valued variables are lower case italics, such as a planet's radius r_p. Vectors containing scalar values are lower case upright bold, such as the vector of coefficients $\mathbf{c}$. Matrices of scalar values are upper case upright bold, such as the matrix of coefficients $\mathbf{G}$. Scalar-valued functions are upper-case italics, such as the potential $V(r, \theta, \phi)$. An exception is the case for a radial position $\tilde{r}(\theta, \phi)$ as function of colatitude θ and longitude ϕ. Vector valued functions mapping to $\mathbb{R}^3$ (radial component, colatitudinal component, and longitudinal component) are lower case bold italics, such as $\boldsymbol{d}(r, \theta, \phi)$. Vectors of scalar valued functions are upper case calligraphic font as for example $\mathcal{Y}$ and matrices of scalar valued functions are upper case bold italics such as $\boldsymbol{A}$. Vectors of vector valued functions are bold calligraphic font such as $\boldsymbol{\mathcal{E}}$. Locations in the three-dimensional space of real numbers are expressed in spherical coordinates as radial coordinate $r > 0$, colatitude $0 \leq \theta \leq \pi$ (0 at the north pole, π at the south pole), and longitude $0 \leq \phi < 2\pi$ with 0 at the prime meridian (fig. 1a). Three-dimensional vector fields are expressed as the projection of

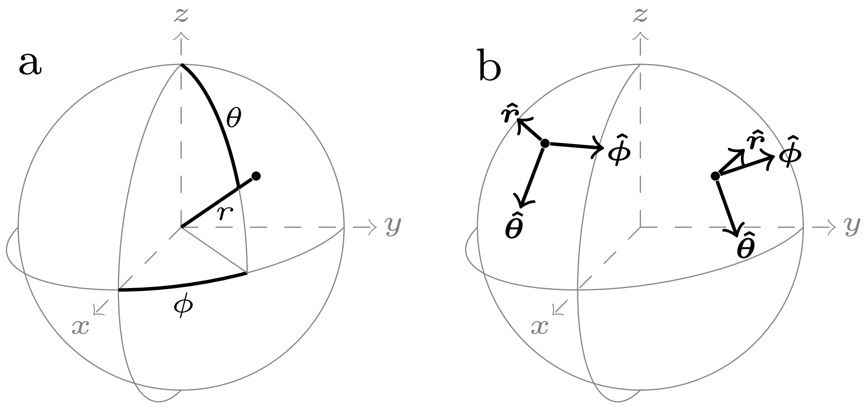

Fig. 1 (a) Spherical coordinate system. Each point in space is described by its radial coordinate $r \geq 0$, colatitude $0 \leq \theta \leq \pi$, and longitude $0 \leq \phi < 2\pi$. Note that the colatitude is $\pi/2-$latitude. (b) Spherical vector components. At each location, a vector is described by its radial (outward) component projected onto the unit vector $\hat{\boldsymbol{r}}$, its colatitudinal (southward) component projected onto the unit vector $\hat{\boldsymbol{\theta}}$ and its longitudinal (eastward) component projected onto the unit vector $\hat{\boldsymbol{\phi}}$.

a vector onto the radial unit vector $\hat{\boldsymbol{r}}$ ("radial component"), the colatitudinal unit vector $\hat{\boldsymbol{\theta}}$ ("colatitudinal component") and the longitudinal unit vector $\hat{\boldsymbol{\phi}}$ ("longitudinal component"), see fig. 1b.

To focus the derivations on the key aspect of this paper — optimally suited functions to analyze potential field data at spacecraft altitude that varies with longitude and colatitude — the specific function spaces are not treated in detail. We assume that they are of sufficient smoothness for the presented calculations. This does not limit the application of the presented approach, because the key functions, such as the radial position as a function of longitude and colatitude, can be chosen to be smooth enough based on the radial positions of the spacecraft data locations, see, e.g., section 4.

The sphere of unit radius is defined as $\Omega := \{(\theta, \phi) \in [0, \pi] \times [0, 2\pi)\}$. This is equivalent to the Cartesian definition $\{(x, y, z) \in \mathbb{R}^3 \mid x^2 + y^2 + z^2 = 1\}$. The integral of a real-valued function F on the unit sphere Ω is

$$\int_\Omega F \, d\Omega = \int_0^{2\pi} \int_0^{\pi} F(\theta, \phi) \sin\theta \, d\theta \, d\phi. \tag{1}$$

The inner product over a subregion of the sphere $R \subseteq \Omega$ of two scalar valued functions is defined as

$$\langle F_1, F_2 \rangle_R := \int_R F_1(\theta, \phi) F_2(\theta, \phi) \, d\Omega \tag{2}$$

and the corresponding norm is

$$|F|_R^2 := \int_R F(\theta, \phi)^2 \, d\Omega \tag{3}$$

The spherical harmonics are

$$Y_{l,m}(\theta,\varphi) = \begin{cases} \sqrt{2} X_{l|m|}(\cos\theta)\cos m\varphi & \text{if } -l \le m < 0, \\ X_{l0}(\cos\theta) & \text{if } m = 0, \\ \sqrt{2} X_{l,m}(\cos\theta)\sin m\varphi & \text{if } 0 < m \le l, \end{cases} \tag{4}$$

where

$$X_{l,m}(\mu) = (-1)^m \left(\frac{2l+1}{4\pi}\right)^{1/2} \left[\frac{(l-m)!}{(l+m)!}\right]^{1/2} \frac{1}{2^l l!}(1-\mu^2)^{m/2} \left(\frac{d}{d\mu}\right)^{l+m} (\mu^2-1)^l \tag{5}$$

for spherical harmonic degree l and order m. A scalar-valued function on the sphere $F : \Omega \to \mathbb{R}$ can be described as a linear combination of spherical harmonics

$$F = \sum_{l=0}^{\infty} \sum_{m=-l}^{l} c_{l,m} Y_{l,m}, \tag{6}$$

where $c_{l,m} \in \mathbb{R}$ for $l \ge 0$ and $-l \le m \le l$ are the spherical harmonic coefficients that describe the function F. Because of the orthonormality of the spherical harmonics with respect to the inner product $\langle \cdot, \cdot \rangle_\Omega$ of eq. (2), these coefficients can be found through $c_{l,m} = \langle F, Y_{l,m} \rangle_\Omega$. This paper considers functions that can be described as a finite linear combination of spherical harmonics with maximum spherical harmonic degree $L_{\max}$

$$F = \sum_{l=0}^{L_{\max}} \sum_{m=-l}^{l} c_{l,m} Y_{l,m}. \tag{7}$$

Such functions are called "bandlimited" in the following. To simplify notations, the $(L_{\max}+1)^2 \times 1$-dimensional vector of spherical harmonics with maximum degree $L_{\max}$ is defined as

$$\mathcal{Y} = \left(Y_{0,0} \ \dots \ Y_{l,m} \ \dots \ Y_{L_{\max},L_{\max}}\right)^\top . \tag{8}$$

The inner product of eq. (2) extends to vectors of functions in an element-wise fashion $\langle \mathcal{Y}, F \rangle_R = \left(\langle Y_{0,0}, F\rangle_R \ \dots \ \langle Y_{L_{\max},L_{\max}}, F\rangle_R\right)^\top$. Therefore, a bandlimited function F can be described as $F = \mathbf{c}^\top \mathcal{Y} = \mathcal{Y}^\top \mathbf{c}$, where $\mathbf{c} = \langle F, \mathcal{Y}\rangle_\Omega = \langle \mathcal{Y}, F\rangle_\Omega$ is the $(L_{\max} + 1)^2 \times 1$-dimensional vector containing the coefficients $c_{l,m} = \langle F, Y_{l,m}\rangle_\Omega = \langle Y_{l,m}, F\rangle_\Omega$. The product of vectors of spherical harmonics is defined as

$$\mathcal{Y}\mathcal{Y}^\top = \begin{pmatrix} Y_{0,0}Y_{0,0} & \cdots & Y_{0,0}Y_{L_{\max},L_{\max}} \\ \vdots & & \vdots \\ Y_{L_{\max},L_{\max}}Y_{0,0} & \cdots & Y_{L_{\max},L_{\max}}Y_{L_{\max},L_{\max}} \end{pmatrix}. \tag{9}$$

The goal is to determine the potential $V(r,\theta,\phi)$ of sources stemming from within a planet from $\boldsymbol{\nabla} V(r,\theta,\phi)$ measured outside of the planet. Such a potential $V(r,\theta,\phi)$

can be approximated by the finite spherical harmonic expansion

$$V(r,\theta,\phi) = \sum_{l=0}^{L_{\max}} \sum_{m=-l}^{l} c_{l,m} \left(\frac{r}{r_p}\right)^{-l-1} Y_{l,m}(\theta,\phi) \tag{10}$$

where r_p is the planet's radius. We note that Plattner and Johnson (2023) accidentally left out the second summation over the spherical harmonic orders m in their eq. (1). The spatial derivative (gradient) can be expressed as $\boldsymbol{\nabla} = \hat{\boldsymbol{r}}\partial_r + r^{-1}\boldsymbol{\nabla_1}$, where $\boldsymbol{\nabla_1} = \hat{\boldsymbol{\theta}}\partial_\theta + \hat{\boldsymbol{\phi}}(\sin\theta)^{-1}\partial_\phi$ denotes the surface gradient on the sphere. Here, the data are assumed to contain solely signals of sources within the planet. If external signals are to be determined simultaneously with internal signals, then the potential field formulation of Plattner and Simons (2017), their eq. (12), should be used. In that case, the derivations presented here can be adapted accordingly. We note that toroidal vector spherical harmonics are not considered here, because we study vector fields that arise as spatial derivatives of a scalar potential $V(r,\theta,\phi)$ and which are therefore irrotational (see, e.g., Blakely, 1995).

Section 3.1 discusses solving for the potential field V of eq. (10) from the radial derivative $\partial_r V$, whereas section 3.2 presents a solution for the potential field V of eq. (10) from all three vector components of the gradient $\boldsymbol{\nabla} V$. For the latter purpose we use the vector spherical harmonics

$$\boldsymbol{e}_{l,m}(\theta,\phi) = \frac{1}{\sqrt{(l+1)(2l+1)}} \left[\hat{\boldsymbol{r}}(l+1)Y_{l,m}(\theta,\phi) - \boldsymbol{\nabla_1} Y_{l,m}(\theta,\phi)\right], \tag{11}$$

where $\boldsymbol{e}_{l,m}(\theta,\phi) : \Omega \to \mathbb{R}^3$. For vector spherical harmonics that are suitable for the expression of contributions of external origin, we again refer to Plattner and Simons (2017). Similar to the scalar-valued spherical harmonics Y_{lm}, the $\boldsymbol{e}_{l,m}(\theta,\phi)$ vector spherical harmonics are collected in an $(L_{\max}+1)^2 \times 1$-dimensional vector of vector valued functions

$$\boldsymbol{\mathcal{E}} = \left(\boldsymbol{e}_{0,0}(\theta,\phi)\ \ldots\ \boldsymbol{e}_{l,m}(\theta,\phi)\ \ldots\ \boldsymbol{e}_{L_{\max},L_{\max}}(\theta,\phi)\right)^\top . \tag{12}$$

The dot product of two vector valued functions $\boldsymbol{f} = \left(f_r\ f_\theta\ f_\phi\right)^\top$ and $\boldsymbol{g} = \left(g_r\ g_\theta\ g_\phi\right)^\top$ is defined as the sum of the product of the components

$$\boldsymbol{f}\cdot\boldsymbol{g} = f_r g_r + f_\theta g_\theta + f_\phi g_\phi, \tag{13}$$

where f_r, f_θ, and f_ϕ are the radial, colatitudinal, and longitudinal components. The inner product of two vector-valued functions $\boldsymbol{f}$ and $\boldsymbol{g}$ over the region R is

$$\langle \boldsymbol{f},\boldsymbol{g}\rangle_R := \int_R \boldsymbol{f}\cdot\boldsymbol{g}\, d\Omega \tag{14}$$

and this definition extends to vectors of vector valued functions, e.g.,

$$\langle \boldsymbol{f}, \boldsymbol{\mathcal{E}} \rangle_R = \left(\langle \boldsymbol{f}, \boldsymbol{e}_{0,0} \rangle_R \ \ldots \ \langle \boldsymbol{f}, \boldsymbol{e}_{L_{\max},L_{\max}} \rangle_R \right)^\top . \tag{15}$$

The vector spherical harmonics $\boldsymbol{e}_{l,m}$ are orthogonal with respect to the inner product over the full sphere $\langle \cdot, \cdot \rangle_\Omega$, meaning that $\langle \boldsymbol{\mathcal{E}}, \boldsymbol{\mathcal{E}}^\top \rangle_\Omega = \mathbf{I}_{(L_{\max}+1)^2}$, where $\mathbf{I}_{(L_{\max}+1)^2}$ is the $(L_{\max}+1)^2 \times (L_{\max}+1)^2$-dimensional unit matrix. This equality does not apply for the inner product over true subregions of the sphere $R \subset \Omega$. Based on the inner product in eq. (14), the norm for functions $\boldsymbol{f} : \Omega \to \mathbb{R}^3$ for a region R is defined as

$$\|\boldsymbol{f}\|_R^2 = \int_R \boldsymbol{f} \cdot \boldsymbol{f} \, d\Omega \tag{16}$$

3 Variable altitude cognizant Slepian functions

The construction of variable altitude cognizant Slepian functions follows the construction of the altitude cognizant Slepian functions of Plattner and Simons (2017) with the key difference that the spacecraft reference radial position in their construction was a scalar constant. Here, the spacecraft reference radial position is a function of longitude and latitude.

3.1 Potential field from radial derivative

To present the key aspect of the construction without the burden of the vectorial notation, this section shows how to construct variable altitude cognizant Slepian functions for the radial derivative of the potential. The second part (section 3.2) presents the derivation for the full three-component spatial derivative (gradient) of the potential. Variable altitude cognizant Slepian functions for internal and external fields can be constructed by combining the approach of section 3.2 with the internal and external approach of Plattner and Simons (2017).

3.1.1 Continuous formulation

We consider the observation $D(r, \theta, \phi)$ of the radial spatial derivative of the potential to be available solely within a spherical region $(\theta, \phi) \in R$. The observations $D(r, \theta, \phi)$ are all outside of the planet, meaning that $r \geq r_p$.

$$D(r, \theta, \phi) = \begin{cases} -\partial_r V(r, \theta, \phi) + N(r, \theta, \phi) & \text{for } (\theta, \phi) \in R \\ \text{unknown} & \text{otherwise.} \end{cases} \tag{17}$$

The noise term $N(r, \theta, \phi)$ also captures signals that do not originate from the inside of the planet, as well as contributions from higher spherical harmonic degrees.

Equation (10) yields that

$$-\partial_r V(r, \theta, \phi) = \sum_{l=0}^{L_{\max}} \sum_{m=-l}^{l} c_{l,m} (l+1) r_p^{-1} \left(\frac{r}{r_p} \right)^{-l-2} Y_{l,m}(\theta, \phi)$$

$$= \mathcal{Y}^\top \boldsymbol{A}\mathbf{c}, \tag{18}$$

where

$$\mathbf{c} = \left(c_{0,0} \; \dots \; c_{l,m} \; \dots \; c_{L_{\max},L_{\max}}\right)^\top, \tag{19}$$

the vector $\mathcal{Y}$ of spherical harmonic functions is defined in eq. (8), and $\boldsymbol{A}$ is an $(L_{\max}+1)^2 \times (L_{\max}+1)^2$ diagonal matrix whose elements are the functions

$$a_l(r) = r_p^{-1}(l+1)(r/r_p)^{-l-2}. \tag{20}$$

In eq. (20), the index l is the spherical harmonic degree of the corresponding column and row of the diagonal element.

The data function of eq. (17) is defined solely within the region R. Our goal is to find the coefficients $\mathbf{c}$ that best fit the data within this region

$$\min_{\mathbf{c}\in\mathbb{R}^{(L_{\max}+1)^2}} |-\partial_r V - D|_R^2. \tag{21}$$

Replacing the radial derivative of the potential with its spherical harmonic expansion eq. (18) and using the definition of the norm of eq. (3) transforms eq. (21) into

$$\begin{aligned}
&\min_{\mathbf{c}\in\mathbb{R}^{(L_{\max}+1)^2}} \left(\int_R \left(\mathbf{c}^\top \boldsymbol{A}\mathcal{Y} - D\right)\left(\mathcal{Y}^\top \boldsymbol{A}\mathbf{c} - D\right)\, d\Omega\right) \\
&= \min_{\mathbf{c}\in\mathbb{R}^{(L_{\max}+1)^2}} \left(\mathbf{c}^\top \int_R \boldsymbol{A}\mathcal{Y}\mathcal{Y}^\top \boldsymbol{A}\, d\Omega\, \mathbf{c} - 2\mathbf{c}^\top \int_R \boldsymbol{A}\mathcal{Y}D\, d\Omega + \int_R D^2\, d\Omega\right) \\
&= \min_{\mathbf{c}\in\mathbb{R}^{(L_{\max}+1)^2}} \left(\mathbf{c}^\top \boldsymbol{K}\mathbf{c} - 2\mathbf{c}^\top \boldsymbol{b} + \int_R D^2\, d\Omega\right)
\end{aligned} \tag{22}$$

where the $(L_{\max}+1)^2 \times (L_{\max}+1)^2$ matrix

$$\boldsymbol{K}(r) = \int_R \boldsymbol{A}(r)\mathcal{Y}\mathcal{Y}^\top \boldsymbol{A}(r)\, d\Omega \tag{23}$$

and the $(L_{\max}+1)^2 \times 1$ vector

$$\boldsymbol{b}(r) = \int_R \boldsymbol{A}(r)\mathcal{Y}D(r,\cdot,\cdot)\, d\Omega \tag{24}$$

contain scalar functions of the radial position r.

To construct Slepian functions following the blueprint of Plattner and Simons (2017), we need to remove the dependence of $\boldsymbol{K}$ on r. Plattner and Simons (2017) achieved this by using a constant value r_s for r in eq. (23). Here, we present a different approach. We use a reference radial position that is a function of longitude and latitude, $r = \tilde{r}(\theta,\phi)$. With such a radial position, the integral over the region R in eq. (23) eliminates the dependence of the matrix $\boldsymbol{K}$ on r and thus yields a matrix of constants, which we denote by $\mathbf{K}$. The same radial position $r = \tilde{r}(\theta,\phi)$ also turns the vector of functions $\boldsymbol{b}$ or eq. (24) into a vector of scalar constants $\mathbf{b}$. For $r = \tilde{r}(\theta, \phi)$, the optimization problem of eq. (21) is thus equivalent to

$$\min_{\mathbf{c}\in\mathbb{R}^{(L_{\max}+1)^2}} \left(\mathbf{c}^\top \mathbf{K}\mathbf{c} - 2\mathbf{c}^\top \mathbf{b} + \gamma\right), \tag{25}$$

where γ is a scalar value that is independent of the coefficients $\mathbf{c}$. Because $\mathbf{K}$ is positive definite (being a Gram matrix), this optimization problem has a single extremum which is a minimum. This minimum can be found by taking the derivative with respect to the coefficients $\mathbf{c}$ and setting the result to zero, yielding

$$\mathbf{K}\,\mathbf{c} = \mathbf{b}. \tag{26}$$

For regions R covering only a fraction of the sphere Ω, eq. (26) tends to be poorly conditioned. To regularize eq. (26), the symmetric positive definite matrix $\mathbf{K}$ can be decomposed into its eigenvectors

$$\mathbf{K} = \mathbf{G}\boldsymbol{\Lambda}\mathbf{G}^\top, \tag{27}$$

where the orthonormal columns $\mathbf{g}_j$ of the matrix $\mathbf{G}$ for $j = 1, \ldots, (L_{\max}+1)^2$ are the eigenvectors of the matrix $\mathbf{K}$ with corresponding eigenvalues λ_i that lie on the diagonal of the matrix $\boldsymbol{\Lambda}$. These eigenvectors are ordered by their eigenvalues in descending order $\lambda_1 \geq \ldots \geq \lambda_{(L_{\max}+1)^2} > 0$. Unlike the eigenvalues for the Slepian function formulation of Simons et al (2006) and Simons and Dahlen (2006), the largest eigenvalue here is not necessarily close to 1. This is a consequence of the scaling introduced by the matrix $\boldsymbol{A}$.

Equation (26) can be regularized by projecting the linear system of equations into the linear space spanned by its eigenvectors corresponding to the J largest eigenvalues. This can be done by replacing $\mathbf{K}$ by its approximation $\mathbf{G}_J\boldsymbol{\Lambda}_J\mathbf{G}_J^\top$. Here, $\mathbf{G}_J$ is the $(L_{\max}+1)^2 \times J$ matrix whose columns are the eigenvectors $\mathbf{g}_1, \ldots, \mathbf{g}_J$ and $\boldsymbol{\Lambda}_J$ is the $J \times J$ diagonal matrix with the eigenvalues $\lambda_1, \ldots, \lambda_J$ on its diagonal. Equation (26) can therefore be approximated by

$$\mathbf{b} = \mathbf{G}\boldsymbol{\Lambda}\mathbf{G}^\top\mathbf{c} \approx \mathbf{G}_J\boldsymbol{\Lambda}_J\mathbf{G}_J^\top\,\bar{\mathbf{c}}, \tag{28}$$

where the $(L_{\max}+1)^2 \times 1$-dimensional vector of spherical harmonic coefficients $\bar{\mathbf{c}}$ is defined as the projection of $\mathbf{c}$ into the space spanned by the orthonormal vectors $\mathbf{g}_1, \ldots, \mathbf{g}_J$

$$\bar{\mathbf{c}} = \mathbf{G}_J\mathbf{G}_J^\top\,\mathbf{c}. \tag{29}$$

The last equality in eq. (28) holds because $\mathbf{G}_J^\top\mathbf{G}_J$ is the $J \times J$ unit matrix. The regularized regional problem is thus to find $\bar{\mathbf{c}}$ such that

$$\mathbf{G}_J\boldsymbol{\Lambda}_J\mathbf{G}_J^\top\,\bar{\mathbf{c}} = \mathbf{b}. \tag{30}$$

For $J < (L_{\max}+1)^2$, eq. (30) is underdetermined because the rank of $\mathbf{G}_J\boldsymbol{\Lambda}_J\mathbf{G}_J^\top$ is J. We consider $\bar{\mathbf{c}}$ the solution of the generalized inverse of eq. (30). The resulting vector

$\bar{\mathbf{c}}$ has a minimal Euclidean norm among all vectors that satisfy eq. (30) and it is also equal to the projection under $\mathbf{G}_J\mathbf{G}_J^\top$ of any vector that satisfies eq. (30).

Definition 1, proposition 1, and remark 1 show how the eigenvectors $\mathbf{G}$ can be used to create functions that regionally approximate $D(r,\theta,\phi)$ to obtain a regional solution for $V(r,\theta,\phi)$.

Definition 1 (radial derivative variable altitude cognizant Slepian functions)**.** *For each eigenvector $\mathbf{g}_j$ of the matrix $\mathbf{K}$ for $j = 1,\ldots,(L_{max}+1)^2$ in eq. (27), the corresponding j-th radial derivative variable altitude cognizant Slepian function is*

$$G'_j(r,\theta,\phi) = \sum_{l=0}^{L_{max}}\sum_{m=-l}^{l}(l+1)g_{l,m;j}r_p^{-1}\left(\frac{r}{r_p}\right)^{-l-2}Y_{l,m}(\theta,\phi), \tag{31}$$

where the $g_{l,m;j}$ are the entries of the eigenvector $\mathbf{g}_j$,

For a choice of an integer $1 \le J \le (L_{max}+1)^2$, the vector containing the functions $G'_j(r,\theta,\phi)$ is

$$\mathcal{G}'_J := \left(G'_1(r,\theta,\phi)\ \ldots\ G'_J(r,\theta,\phi)\right)^\top = \mathbf{G}_J^\top \boldsymbol{A}\mathcal{Y}. \tag{32}$$

The corresponding potential variable altitude cognizant Slepian functions are

$$G_j(r,\theta,\phi) = \sum_{l=0}^{L_{max}}\sum_{m=-l}^{l} g_{l,m;j}\left(\frac{r}{r_p}\right)^{-l-1}Y_{l,m}(\theta,\phi), \tag{33}$$

and the vector containing the $G_j(r_p,\theta,\phi)$, evaluated at the planet's reference radius r_p, is

$$\mathcal{G}_J = \left(G_1(r_p,\theta,\phi)\ \ldots\ G_J(r_p,\theta,\phi)\right)^\top = \mathbf{G}_J^\top\mathcal{Y}. \tag{34}$$

Proposition 1. *For any choice of integer $1 \le J \le (L_{max}+1)^2$, the spherical harmonic coefficients $\bar{\mathbf{c}}$ of eq. (28) can be calculated from the inner products $\langle G'_j(\tilde{r}(\theta,\phi),\theta,\phi), D(\tilde{r}(\theta,\phi),\theta,\phi)\rangle_R$ of the data function D with the radial derivative variable altitude cognizant Slepian functions G'_j of definition 1. Specifically,*

$$\bar{\mathbf{c}} = \mathbf{G}_J\boldsymbol{\Lambda}_J^{-1}\langle\mathcal{G}'_J, D\rangle_R, \tag{35}$$

where $\mathbf{G}_J$ is the matrix of eigenvectors from eq. (28).

Proof. Multiply both sides of eq. (30) from the left with $\mathbf{G}_J^\top$, which is the left inverse of $\mathbf{G}_J$, and use eq. (24) and definition 1 to obtain

$$\boldsymbol{\Lambda}_J\mathbf{G}_J^\top\bar{\mathbf{c}} = \int_R \mathbf{G}_J^\top\boldsymbol{A}\mathcal{Y}D\,d\Omega = \langle\mathcal{G}'_J, D\rangle_R. \tag{36}$$

Equation (35) follows from the definition of $\boldsymbol{\Lambda}_J$ as a diagonal matrix with positive eigenvalues, which is invertible. Finally, $\bar{\mathbf{c}}$ is equal to the projection of $\bar{\mathbf{c}}$ under the projection operator $\mathbf{G}_J\mathbf{G}_J^\top$, meaning $\mathbf{G}_J\mathbf{G}_J^\top\bar{\mathbf{c}} = \bar{\mathbf{c}}$. □

Remark 1. *The coefficients* $\mathbf{s}_J := \mathbf{G}_J^\top \bar{\mathbf{c}} = \mathbf{\Lambda}_J^{-1} \langle \mathcal{G}'_J, D \rangle_R$ *expanded in the basis* $\mathcal{G}_J$ *represent the potential field within the region* R *on the planet's surface* $r = r_p$,

$$(\mathcal{G}_J)^\top \mathbf{s}_J = \mathcal{Y}^\top \mathbf{G}_J \mathbf{G}_J^\top \bar{\mathbf{c}} = \mathcal{Y}^\top \bar{\mathbf{c}} \approx \mathcal{Y}^\top \mathbf{c} = V(r_p, \theta, \phi) \tag{37}$$

In remark 1, the second equality holds because $\bar{\mathbf{c}}$ is equal to the projection of $\bar{\mathbf{c}}$ under the projection operator $\mathbf{G}_J \mathbf{G}_J^\top$, the approximation holds because of the regularization in eq. (28), and the last equality follows from eq. (10).

The following examples show the difference between the variable altitude cognizant Slepian functions of eq. (33) and the fixed altitude cognizant Slepian functions of Plattner and Simons (2017), as well as the classical Slepian functions of Simons et al (2006) and Simons and Dahlen (2006). These examples of each type of Slepian function are constructed for the region R = Africa, r_p = 6371 km and maximum spherical harmonic degree $L_{\max} = 60$. For the variable altitude cogizant Slepian functions, the radial position $r = \tilde{r}(\theta, \phi)$ follows a prolate rotational ellipsoid aligned with Earth's spin axis with semi-diameter $1.04\, r_p$ in the equatorial plane and semi-diameter $1.1\, r_p$ along the spin axis. This ellipsoid is shifted northward along the spin axis by $0.09\, r_p$ (fig. 2a). The planet's radius is r_p = 6371 km, the radius of the Earth. Across the region R = Africa, the spacecraft altitude $r - r_p$ ranges from 102 km to 1535 km with the lowest altitude at the southern tip of the continent. The average spacecraft altitude over R = Africa is $r - r_s$ = 607 km. We use r_s = 6978 km as the reference radial position for the construction of the fixed altitude cognizant Slepian functions. The classical Slepian functions do not depend on a spacecraft altitude.

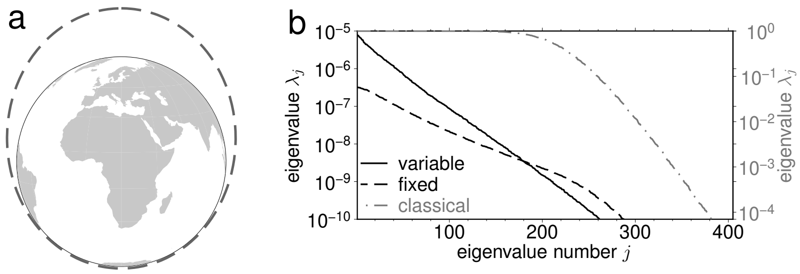

Fig. 2 (a) Orbit for example functions (dashed line). Orbit is axisymmetric with respect to Earth's spin axis. (b) Eigenvalues for the three types of Slepian functions of fig. 3 — classical Slepian functions (R = Africa, $L_{\max} = 60$), fixed altitude cognizant Slepian functions (r_s = 6978 km), and variable altitude cognizant Slepian functions ($r = \tilde{r}(\theta, \phi)$ given by the ellipsoid in (a) and defined in the main text).

The eigenvalues corresponding to the variable altitude cognizant Slepian functions (eq. 27) indicate their relative suitability to solve eq. (21). Unlike the eigenvalues of the classical Slepian functions, which are between 0 and 1 (Simons et al, 2006; Simons and Dahlen, 2006), the eigenvalues of variable altitude cognizant Slepian functions contain the downward continuation factor (eqs. 20 and 23) and thus typically have small but positive values. Plattner and Simons (2017) observed a similar pattern for the fixed altitude cognizant Slepian funcitons. In our example for R = Africa, $L_{\max} = 60$, and $r = \tilde{r}(\theta, \phi)$ following an ellipsis (fig. 2a), the variable altitude cognizant Slepian functions have a few eigenvalues that are greater than the corresponding eigenvalues of the fixed altitude cognizant Slepian functions, but the eigenvalue slope of the variable altitude cognizant Slepian functions is steeper than the eigenvalue slope of the fixed altitude cognizant Slepian functions (fig. 2b). This is to be expected, because some of the variable altitude cognizant Slepian functions are constructed for lower altitudes and thus have better conditioning under downward continuation. On the other hand, all fixed altitude cognizant Slepian functions are constructed for the same altitude and thus can not make use of the lower altitude over southern Africa. The eigenvalues of the classical Slepian functions show a pronounced step from a few eigenvalues close to 1 to eigenvalues close to 0, as observed by Simons et al (2006) and Simons and Dahlen (2006).

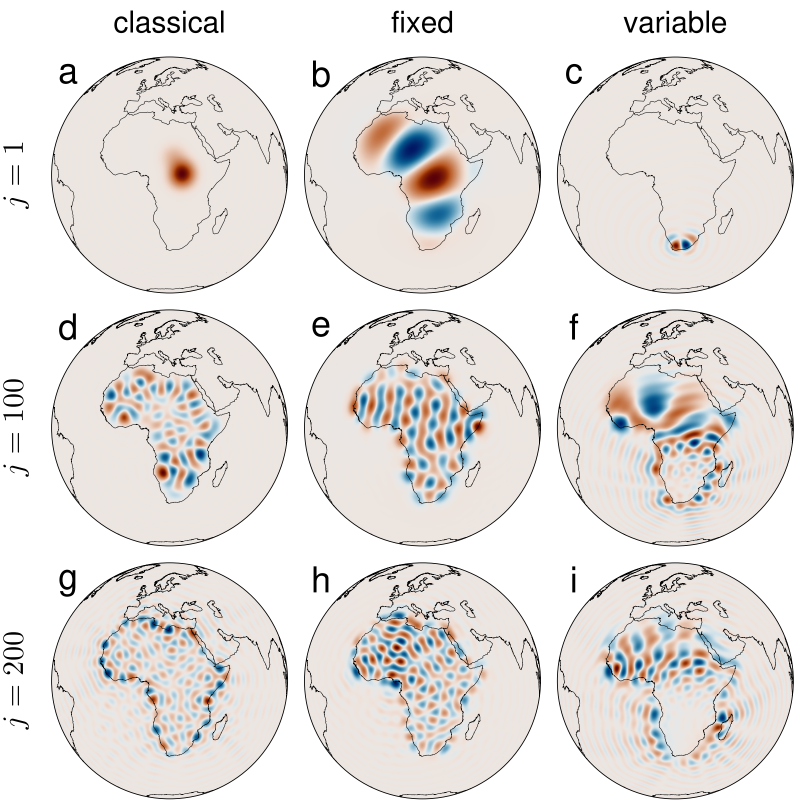

Fig. 3 Classical Slepian functions, altitude-cognizant Slepian functions, and variable altitude cognizant Slepian functions for $L_{\max} = 60$, $R =$ Africa and reference radial position $r = \tilde{r}(\theta, \phi)$ given by the the elliptical orbit in fig. 2a.

Comparing the spatial patterns of the classical Slepian functions constructed for $R =$ Africa, $L_{\max} = 60$, (fig. 3a,d,g) with the spatial pattern of the fixed altitude cognizant Slepian functions for the same region R and $L_{\max}$, but altitude 607 km above the reference radius of 6371 km (fig. 3b,e,h) shows that the classical Slepian functions tend to better focus their energy within the region, whereas the fixed altitude cognizant Slepian functions balance spatial concentration with conditioning of solving for the coefficients $\mathbf{c}$ of the potential $V(r,\theta,\phi)$ on the planet's surface (eq. 18). The variable altitude cognizant Slepian functions (fig. 3c,f,i) for reference radial position $r = \tilde{r}(\theta,\phi)$ (fig. 2a), region R = Africa and $L_{\max} = 60$ resolve the region R depending on the ellipsoid height given by $r = \tilde{r}(\theta,\phi)$. For low indices j, the variable altitude cognizant Slepian functions focus on the southern tip of the region R, where the ellipsoid is closest to the planet. Functions for higher indices resolve areas where the ellipsoid is farther away from the planet's surface.

3.1.2 Discrete formulation

In geophysical applications, $D(r,\theta,\phi)$, is recorded at a finite number n of locations (r_k,θ_k,ϕ_k) for $k = 1,\ldots,n$. This yields a vector

$$\mathbf{d} = \big(D(r_1,\theta_1,\phi_1)\ \ldots\ D(r_n,\theta_n,\phi_n)\big)^\top \in \mathbb{R}^n \tag{38}$$

for which we seek to obtain the spherical harmonic coefficients $\mathbf{c}$ that represent the continuous potential field (eq. 10). These coefficients can be calculated using the spherical harmonics upward continued to the individual data locations

$$\mathbf{Z}^\top \mathbf{c} = \mathbf{d}, \tag{39}$$

where the elements of the matrix $\mathbf{Z}$ are

$$Z_{l,m;k} = a_l(r_k) Y_{l,m}(\theta_k,\phi_k), \tag{40}$$

for $(l,m) = (0,0),\ldots,(L_{\max},L_{\max})$ and $k = 1,\ldots,n$. The upward continuation factor $a_l(r)$ is defined in eq. (20).

When measurement locations (r_k,θ_k,ϕ_k) for $k = 1,\ldots,n$ are available within a spatially confined region R only, then the linear system of equations (eq. 39) is poorly conditioned. To regularize eq. (39), the J best-suited variable altitude cognizant Slepian functions of definition 1 can be used instead of the spherical harmonics. The value for J, the number of Slepian functions to use, controls the trade off between resolution of the potential and amplification of short spatial scales under downward continuation. J is thus a regularization parameter that is problem dependent. Plattner and Johnson (2023) provide a strategy for choosing J. The regularized regional problem is

$$\mathbf{M}_J^\top \mathbf{s}_J = \mathbf{d}, \tag{41}$$

where the elements of the $J \times n$ matrix $\mathbf{M}_J$ are

$$M_{j;k} = G'_j(r_k,\theta_k,\phi_k), \tag{42}$$

thus, $\mathbf{M}_J^\top = \mathbf{G}_J^\top \mathbf{Z}$. From the coefficients $\mathbf{s}_J$ in eq. (41), the locally representative spherical harmonic coefficients $\bar{\mathbf{c}}$ can be calculated using the same transformation as for the continuous case $\bar{\mathbf{c}} = \mathbf{G}_J \mathbf{s}_J$. The linear system of equations (41) can be solved using a least squares approach, or using an iteratively reweighted least squares approach (e.g., Farquharson and Oldenburg, 1998). The least squares formulation is

$$(\mathbf{M}_J \mathbf{M}_J^\top)\mathbf{s}_J = \mathbf{M}_J \mathbf{d}. \tag{43}$$

Solving eq. (43) is the discrete counterpart to inverting the matrix $\mathbf{\Lambda}_J$ in proposition 1. In fact, eq. (43) is a discretized approximation of eq. (36) because the entries of $\mathbf{Z}\mathbf{Z}^\top$ are

$$\begin{aligned}(\mathbf{Z}\mathbf{Z}^\top)_{l,m;l',m'} &= \sum_{k=1}^{n} a_l(r_k) a_{l'}(r_k) Y_{l,m}(\theta_k,\phi_k) Y_{l',m'}(\theta_k,\phi_k) &(44)\\ &\approx n \int_R a_l a_{l'} Y_{l,m} Y_{l',m'}\, d\Omega &(45)\\ &= n \left(\int_R \boldsymbol{A}\mathcal{Y}\mathcal{Y}^\top \boldsymbol{A}\, d\Omega \right)_{l,m;l',m'} \\ &= n\, \mathbf{K}_{l,m;l',m'}.\end{aligned}$$

Therefore, $\mathbf{M}_J\mathbf{M}_J^\top = \mathbf{G}_J^\top \mathbf{Z}\mathbf{Z}^\top \mathbf{G}_J \approx n\mathbf{G}_J^\top \mathbf{K} \mathbf{G}_J = n\mathbf{G}_J^\top \mathbf{G}_J \mathbf{\Lambda}_J \mathbf{G}_J^\top \mathbf{G}_J = n\mathbf{\Lambda}_J$. Analogously,

$$\begin{aligned}(\mathbf{M}_J\mathbf{d})_j &= \sum_{k=1}^{n} \sum_{l=0}^{L_{max}} \sum_{m=-l}^{l} g_{l,m;j}\, a_l(r_k) Y_{l,m}(\theta_k,\phi_k) D(\theta_k,\phi_k) \\ &\approx n \sum_{l=0}^{L_{max}} \sum_{m=-l}^{l} g_{l,m;j} \int_R a_l\, Y_{l,m}\, D\, d\Omega &(46)\\ &= n\left(\langle \mathcal{G}'_J, D\rangle_R\right)_j.\end{aligned}$$

The approximations in eq. (45) and (46) hold true only if $r_k \approx r(\theta_k, \phi_k)$ and if (θ_k, ϕ_k, r_k) are equidistributed within the region R. Otherwise, the data points need to be weighted by replacing $\mathbf{Z}$ by $\mathbf{ZW}$ and $\mathbf{d}$ by $\mathbf{Wd}$, where $\mathbf{W} \in \mathbb{R}^{n\times n}$ is a diagonal matrix with entries w_k that reflect the weights of a suitable numerical integration scheme.

Figure 4 presents a comparison of the eigenvalues λ_j, $j = 1, \ldots, J$. Here, only the first $J = 300$ eigenvalues are shown of the variable altitude cognizant Slepian functions in fig. 3c,f,e with $\mathbf{M}\mathbf{M}^\top/n$ for $n = 10000$ randomly distributed data locations in $R =$ Africa. The radial position of the random data locations are on the ellipsoid $\tilde{r}(\theta, \phi)$ of fig. 2a with an added normally distributed random offset of r_{rand} and ensuring that no radial position is less than $r_p = 6371$ km. For all data locations perfectly located on the ellipsis ($r_{\text{rand}} = 0$), the matrix $\mathbf{M}\mathbf{M}^\top/n$ is nearly diagonal (fig. 4a) and its diagonal values closely follow the eigenvalues λ_j (fig. 4d). With increasing r_{rand}, the off diagonal elements of $\mathbf{M}\mathbf{M}^\top/n$ increase (fig. 4b,c), and the diagonal elements differ increasingly from λ_j (fig. 4d).

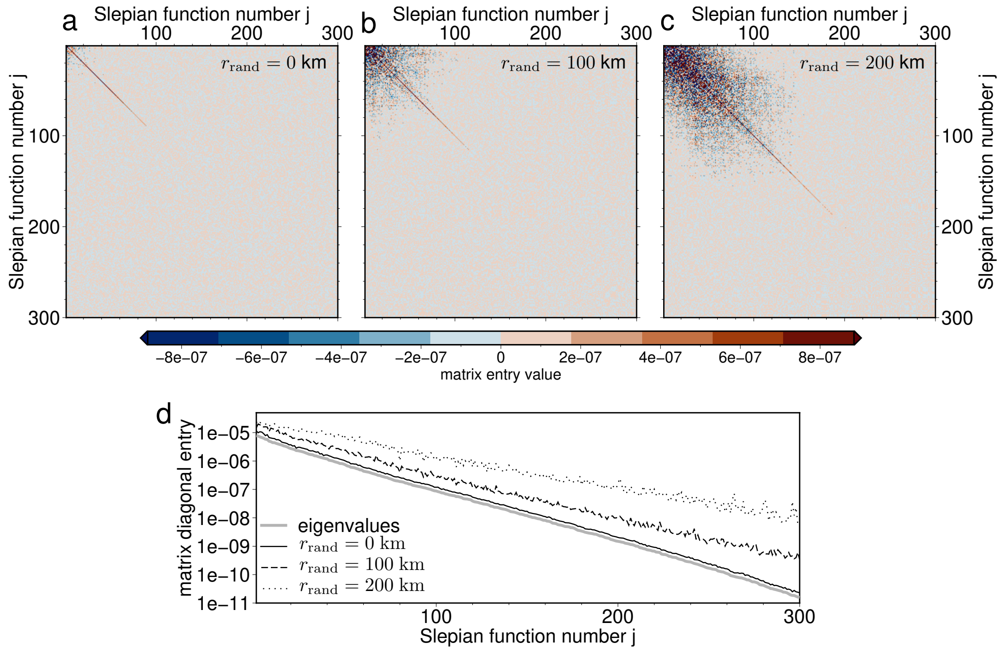

Fig. 4 Comparison of $\mathbf{M}\mathbf{M}^\top/n$ to $\mathbf{\Lambda}_J$ for the variable altitude cognizant Slepian functions of fig. 3c,f,e for $n = 10000$ randomly distributed points over $R =$ Africa with radial position randomly offset from the ellipsoid $\tilde{r}(\theta, \phi)$ of fig. 2a. The random radial offset is normally distributed with standard deviation $r_{\rm rand}$, and minimal radial position $r_p = 6371$ km. Panels show $\mathbf{M}\mathbf{M}^\top/n$ for (a) $r_{\rm rand} = 0$ km, (b) $r_{\rm rand} = 100$ km, and (c) $r_{\rm rand} = 200$ km. (d) Eigenvalues λ_j for $1 \le j \le 300$ and diagonal elements of panels a, b, and c.

3.2 Potential field from radial, colatitudinal, and longitudinal derivatives

The construction of the variable altitude cognizant Slepian functions for all three components of the spatial derivative follows the approach of section 3.1 with the added complexity of a three-dimensional image space.

3.2.1 Continuous formulation

As for section 3.1.1, the goal is to solve for a potential field $V(r, \theta, \phi)$ of eq. (10) given a data function

$$\boldsymbol{d}(r, \theta, \phi) = \begin{cases} -\boldsymbol{\nabla} V(r, \theta, \phi) + \boldsymbol{n}(r, \theta, \phi) & \text{for } (\theta, \phi) \in R \\ \text{unknown} & \text{otherwise,} \end{cases} \tag{47}$$

where the noise function $\boldsymbol{n}(\cdot,\cdot,r)$ maps into $\mathbb{R}^3$ given as the radial, longitude, and colatitude component. The spatial gradient of $V(r,\theta,\phi)$ can be expressed as

$$\begin{aligned} -\boldsymbol{\nabla} V(r,\theta,\phi) &= \sum_{l=0}^{L_{\max}} \sum_{m=-l}^{l} c_{l,m} \sqrt{(l+1)(2l+1)} r_p^{-1} \left(\frac{r}{r_p}\right)^{-l-2} \boldsymbol{e}_{l,m}(\theta,\phi), \\ &= \boldsymbol{\mathcal{E}}^\top \dot{\boldsymbol{A}} \mathbf{c}, \end{aligned} \tag{48}$$

where $\mathbf{c}$ is defined in eq. (19) and $\boldsymbol{\mathcal{E}}$ in eq. (12). The matrix $\dot{\boldsymbol{A}}$ is an $(L_{\max}+1)^2 \times (L_{\max}+1)^2$ diagonal matrix whose diagonal elements are

$$\dot{a}_l(r) = \sqrt{(l+1)(2l+1)} r_p^{-1} \left(\frac{r}{r_p}\right)^{-l-2}, \tag{49}$$

where l is the spherical harmonic degree of the corresponding column and row.

As for section 3.1.1, our goal is to find the coefficients $\mathbf{c}$ such that the misfit between the gradient of the potential and the data function is minimized

$$\min_{\mathbf{c}\in\mathbb{R}^{(L_{\max}+1)^2}} \|-\boldsymbol{\nabla} V - \boldsymbol{d}\|_R^2 \tag{50}$$

Replacing $-\boldsymbol{\nabla} V$ using eq. (48) and the definition of the norm in eq. (16) yields

$$\min_{\mathbf{c}\in\mathbb{R}^{(L_{\max}+1)^2}} \|-\boldsymbol{\nabla} V - \boldsymbol{d}\|_R^2 \tag{51}$$

$$= \min_{\mathbf{c}\in\mathbb{R}^{(L_{\max}+1)^2}} \left(\int_R \left(\mathbf{c}^\top \dot{\boldsymbol{A}} \boldsymbol{\mathcal{E}} - \boldsymbol{d}\right) \cdot \left(\boldsymbol{\mathcal{E}}^\top \dot{\boldsymbol{A}} \mathbf{c} - \boldsymbol{d}\right) d\Omega \right) \tag{52}$$

$$= \min_{\mathbf{c}\in\mathbb{R}^{(L_{\max}+1)^2}} \left(\mathbf{c}^\top \int_R \dot{\boldsymbol{A}} (\boldsymbol{\mathcal{E}} \cdot \boldsymbol{\mathcal{E}}^\top) \dot{\boldsymbol{A}} \, d\Omega \, \mathbf{c} - 2\mathbf{c}^\top \int_R \dot{\boldsymbol{A}} \boldsymbol{\mathcal{E}} \cdot \boldsymbol{d} \, d\Omega + \int_R \boldsymbol{d} \cdot \boldsymbol{d} \, d\Omega \right) \tag{53}$$

$$= \min_{\mathbf{c}\in\mathbb{R}^{(L_{\max}+1)^2}} \left(\mathbf{c}^\top \dot{\boldsymbol{K}} \mathbf{c} - 2\mathbf{c}^\top \dot{\boldsymbol{b}} + \int_R \boldsymbol{d} \cdot \boldsymbol{d} \, d\Omega \right), \tag{54}$$

where we defined the $(L_{\max}+1)^2 \times (L_{\max}+1)^2$ matrix

$$\dot{\boldsymbol{K}}(r) = \int_R \dot{\boldsymbol{A}}(r) (\boldsymbol{\mathcal{E}} \cdot \boldsymbol{\mathcal{E}}^\top) \dot{\boldsymbol{A}}(r) \, d\Omega \tag{55}$$

and the $(L_{\max}+1)^2 \times 1$ vector

$$\dot{\boldsymbol{b}}(r) = \int_R \dot{\boldsymbol{A}}(r) (\boldsymbol{\mathcal{E}} \cdot \boldsymbol{d}(r,\cdot,\cdot)) \, d\Omega. \tag{56}$$

As for the radial case in section 3.1.1, if we use a radial position that is a function of longitude and latitude $r = \tilde{r}(\theta,\phi)$, then the matrix $\dot{\boldsymbol{K}}$ in eq. (55) contains scalar constants. We thus denote it using an upright font $\dot{\mathbf{K}}$. In this case, eq. (50) is equivalent to

$$\min_{\mathbf{c}\in\mathbb{R}^{(L_{\max}+1)^2}} \left(\mathbf{c}^\top\dot{\mathbf{K}}\mathbf{c} - 2\mathbf{c}^\top\dot{\mathbf{b}} + \gamma\right), \tag{57}$$

where γ is a scalar independent of the coefficients $\mathbf{c}$. Because $\dot{\mathbf{K}}$ is symmetric positive definite, this optimization problem has a single extremum which is a minimum. This minimum can be found by taking the derivative with respect to the coefficients $\mathbf{c}$ and setting the result to zero. This yields

$$\dot{\mathbf{K}}\,\mathbf{c} = \dot{\mathbf{b}}. \tag{58}$$

For true subregions of the sphere $R \subset \Omega$, eq. (58) is poorly conditioned. We use the eigenvector decomposition of the symmetric positive definite matrix $\dot{\mathbf{K}}$

$$\dot{\mathbf{K}} = \dot{\mathbf{G}}\dot{\mathbf{\Lambda}}\dot{\mathbf{G}}^\top, \tag{59}$$

of which the $(L_{\max}+1)^2$ eigenvectors $\dot{\mathbf{g}}_j, j = 1, \ldots, (L_{\max}+1)^2$ in the matrix $\dot{\mathbf{G}}$ are ordered based on their eigenvalues $\dot{\lambda}_1 \geq \ldots \geq \dot{\lambda}_{(L_{\max}+1)^2} > 0$ and the diagonal matrix $\dot{\mathbf{\Lambda}}$ contains the eigenvalues $\dot{\lambda}_1, \ldots, \dot{\lambda}_{(L_{\max}+1)^2}$. To regularize eq. (59), the matrix $\dot{\mathbf{K}}$ can be replaced by $\dot{\mathbf{G}}_J\dot{\mathbf{\Lambda}}_J\dot{\mathbf{G}}_J^\top$, where the columns of the $(L_{\max}+1)^2 \times J$-dimensional matrix $\dot{\mathbf{G}}_J$ are the eigenvectors $\dot{\mathbf{g}}_j$ for $j = 1, \ldots, J$, and the $J \times J$-dimensional diagonal matrix $\dot{\mathbf{\Lambda}}_J$ contains the corresponding eigenvalues $\dot{\lambda}_j$. The dimension of the projection space J is a regularization parameter for which the choice depends on the problem and the data function $\boldsymbol{d}(r,\theta,\phi)$ of eq. (47). This regularized problem is

$$\dot{\mathbf{b}} = \dot{\mathbf{G}}\dot{\mathbf{\Lambda}}\dot{\mathbf{G}}^\top\mathbf{c} \approx \dot{\mathbf{G}}_J\dot{\mathbf{\Lambda}}_J\dot{\mathbf{G}}_J^\top\bar{\mathbf{c}}, \tag{60}$$

where the regionally representative spherical harmonic coefficients $\bar{\mathbf{c}}$ are a projection of the spherical harmonic coefficients $\mathbf{c}$ into the space spanned by the orthonormal vectors $\dot{\mathbf{g}}_1, \ldots, \dot{\mathbf{g}}_J$

$$\bar{\mathbf{c}} = \dot{\mathbf{G}}_J\dot{\mathbf{G}}_J^\top\mathbf{c}. \tag{61}$$

The following definition 2, proposition 2, and remark 2 show how three-dimensional vector valued variable altitude cognizant Slepian functions can be constructed so that they can solve for spherical harmonic coefficients which represent the potential field $V(r,\theta,\phi)$ within the region of data availability.

Definition 2 (vector derivative variable altitude cognizant Slepian functions)**.** *For each eigenvector $\dot{\mathbf{g}}_j$ of matrix $\dot{\mathbf{K}}$ in eq. (59), the corresponding j-th vector derivative variable altitude cognizant Slepian functions is*

$$\dot{\boldsymbol{G}}_j'(r,\theta,\phi) = \sum_{l=0}^{L_{max}}\sum_{m=-l}^{l} \dot{g}_{l,m;j}\sqrt{(l+1)(2l+1)}\,r_p^{-1}\left(\frac{r}{r_p}\right)^{-l-2}\boldsymbol{e}_{l,m}(\theta,\phi), \tag{62}$$

where the $\dot{g}_{l,m;j}$ are the entries of the eigenvector $\dot{\mathbf{g}}_j$ for a $1 \leq j \leq (L_{max}+1)^2$

For a choice of integer $1 \leq J \leq (L_{max}+1)^2$, the vector containing the functions $\dot{\boldsymbol{G}}'_j$ ordered by their corresponding eigenvalues λ_1 in decreasing order is

$$\dot{\boldsymbol{\mathcal{G}}}'_J := \left(\dot{\boldsymbol{G}}'_1(r,\theta,\phi) \ \ldots \ \dot{\boldsymbol{G}}'_J(r,\theta,\phi)\right)^\top = \dot{\mathbf{G}}_J^\top \dot{\boldsymbol{A}}\boldsymbol{\mathcal{E}}. \tag{63}$$

The corresponding potential variable altitude cognizant Slepian functions are

$$\dot{G}_j = \sum_{l=0}^{L_{max}} \sum_{m=-l}^{l} \dot{g}_{l,m;j} \left(\frac{r}{r_p}\right)^{-l-1} Y_{l,m}(\theta,\phi), \tag{64}$$

and the vector containing the $\dot{G}_j(r_p,\theta,\phi)$, evaluated at the planet's reference radius r_p, is

$$\dot{\mathcal{G}}_J = \left(\dot{G}_1(r_p,\theta,\phi) \ \ldots \ \dot{G}_J(r_p,\theta,\phi)\right)^\top = \dot{\mathbf{G}}_J^\top \mathcal{Y}. \tag{65}$$

Proposition 2. *For any choice of integer $1 \leq J \leq (L_{max}+1)^2$, the spherical harmonic coefficients $\bar{\mathbf{c}}$ of eq. (60) can be calculated from the inner products $\langle \dot{\boldsymbol{G}}'_j(\tilde{r}(\theta,\phi),\theta,\phi), \boldsymbol{d}(\tilde{r}(\theta,\phi),\theta,\phi)\rangle_R$ of the data function $\boldsymbol{d}$ with the radial derivative variable altitude cognizant Slepian functions $\dot{\boldsymbol{G}}'_j(r,\theta,\phi)$ of definition 2. Specifically,*

$$\bar{\mathbf{c}} = \dot{\mathbf{G}}_J \dot{\boldsymbol{\Lambda}}_J^{-1} \langle \dot{\boldsymbol{\mathcal{G}}}'_J, \boldsymbol{d}\rangle_R, \tag{66}$$

where $\dot{\mathbf{G}}_J$ is the matrix of eigenvectors from eq. (60).

Proof. The proof for the three component derivative case follows the same steps as for the radial case in proposition 1 mutatis mutandis. □

Remark 2. *The coefficients $\mathbf{s}_J := \dot{\mathbf{G}}_J^\top \bar{\mathbf{c}}$ expanded in the basis $\dot{\mathcal{G}}_J$ represent the potential field within the region R,*

$$(\dot{\mathcal{G}}_J)^\top \mathbf{s}_J = \mathcal{Y}^\top \dot{\mathbf{G}}_J \dot{\mathbf{G}}_J^\top \bar{\mathbf{c}} = \mathcal{Y}^\top \bar{\mathbf{c}} \approx \mathcal{Y}^\top \mathbf{c} = V(r,\theta,\phi). \tag{67}$$

3.2.2 Discrete formulation

Spacecraft measurements of the data $\boldsymbol{d}(r,\theta,\phi)$ are recorded as discrete values at a finite number n of data locations (r_k,θ_k,ϕ_k) for $k=1,\ldots,n$. These measurements can be collected in a $3n$-dimensional vector

$$\dot{\mathbf{d}} = \left(\dot{\mathbf{d}}_r^\top \ \dot{\mathbf{d}}_\theta^\top \ \dot{\mathbf{d}}_\phi^\top\right)^\top \in \mathbb{R}^{3n}, \tag{68}$$

where

$$\begin{aligned}
\dot{\mathbf{d}}_r &= \left(\boldsymbol{d}_r(r_1,\theta_1,\phi_1) \ \ldots \ \boldsymbol{d}_r(r_n,\theta_n,\phi_n)\right)^\top \in \mathbb{R}^n,\\
\dot{\mathbf{d}}_\theta &= \left(\boldsymbol{d}_\theta(r_1,\theta_1,\phi_1) \ \ldots \ \boldsymbol{d}_\theta(r_n,\theta_n,\phi_n)\right)^\top \in \mathbb{R}^n,
\end{aligned}$$

$$\dot{\mathbf{d}}_\phi = \left(\boldsymbol{d}_\phi(r_1, \theta_1, \phi_1) \ \ldots \ \boldsymbol{d}_\phi(r_n, \theta_n, \phi_n)\right)^\top \in \mathbb{R}^n.$$

Here, $\boldsymbol{d}_r(r_k, \theta_k, \phi_k)$ is the radial component of the vector-valued function $\boldsymbol{d}_r$ at the data location (r_k, θ_k, ϕ_k) for $k = 1, \ldots, n$ and $\boldsymbol{d}_\theta$ and $\boldsymbol{d}_\phi$ are the colatitudinal and longitudinal components, respectively. From these data, the goal is to determine spherical harmonic coefficients $\mathbf{c}$ such that

$$\dot{\mathbf{Z}}^\top \mathbf{c} = \dot{\mathbf{d}}, \tag{69}$$

where

$$\dot{\mathbf{Z}} = \left(\dot{\mathbf{Z}}_r^\top \ \dot{\mathbf{Z}}_\theta^\top \ \dot{\mathbf{Z}}_\phi^\top\right)^\top. \tag{70}$$

The elements of the $(L_{\text{max}} + 1)^2 \times n$-dimensional matrix $\dot{\mathbf{Z}}_r$ are

$$\left[\dot{Z}_{l,m;k}\right]_r = \dot{a}_l(r_k) \left[\boldsymbol{e}_{l,m}(\theta_k, \phi_k)\right]_r, \tag{71}$$

where $(\boldsymbol{e}_{l,m}(\theta_k, \phi_k))_r$ is the radial component of the vector-valued function $\boldsymbol{e}_{l,m}$ of eq. (11) evaluated at the location (θ_k, ϕ_k). The elements of $\dot{\mathbf{Z}}_\theta$ and $\dot{\mathbf{Z}}_\theta$ are defined as

$$\left[\dot{Z}_{l,m;k}\right]_\theta = \dot{a}_l(r_k) \left[\boldsymbol{e}_{l,m}(\theta_k, \phi_k)\right]_\theta \quad \text{and} \quad \left[\dot{Z}_{l,m;k}\right]_\phi = \dot{a}_l(r_k) \left[\boldsymbol{e}_{l,m}(\theta_k, \phi_k)\right]_\phi, \tag{72}$$

respectively. The upward continuation factor $\dot{a}_l$ is defined in eq. (49).

If the data locations (θ_k, ϕ_k) for $k = 1, \ldots, n$ are available only within a subregion R of the sphere Ω, then the linear system of equations (69) may become poorly conditioned. To regularize eq. (69) we use the J best-suited variable altitude cognizant Slepian functions of definition 2. The value for J, the number of Slepian functions to use, controls the tradeoff between resolving short spatial scales in the data and amplifying noise under downward continuation. Plattner and Johnson (2023) present a strategy to choose a suitable value for J. The local regularized linear system of equations is

$$\dot{\mathbf{M}}_J^\top \mathbf{s}_J = \dot{\mathbf{d}}, \tag{73}$$

where $\dot{\mathbf{M}}_J = \dot{\mathbf{G}}_J^\top \dot{\mathbf{Z}}$. The linear system of equations (73) can be solved using a least squares approach, or using an iteratively reweighted least squares approach (e.g., Farquharson and Oldenburg, 1998). The regionally-representative spherical harmonic coefficients $\bar{\mathbf{c}}$ can be obtained from the coefficient vector $\mathbf{s}_J$ of eq. (73) using the matrix $\dot{\mathbf{G}}_J$

$$\bar{\mathbf{c}} = \dot{\mathbf{G}}_J \mathbf{s}_J. \tag{74}$$

In section 3.1.2 we present a comparison between the analytical formulation of eq. (36) and the discrete formulation of eq. (43) for the radial derivative case. A similar relationship can be derived for the full vectorial case presented in this section.

4 Numerical experiments

The following numerical experiments highlight a situation in which variable altitude cognizant Slepian functions (section 3.1, section 3.2) outperform the fixed altitude cognizant Slepian functions (Plattner and Simons, 2017) as well as the classical Slepian functions (Simons et al, 2006; Simons and Dahlen, 2006). We create random spherical harmonic coefficients $c_{l,m}$ for $l = 1, \ldots, L_{\max}$ and $m = -l, \ldots, l$ which we collect in a vector $\mathbf{c}_{\mathrm{True}}$. We consider these coefficients to represent the "true" potential (fig. 5) that we aim to recover from noisy data collected at spacecraft altitude. For each spherical harmonic degree l the $c_{l,m}$ are Gaussian randomly distributed and their power per degree $(l+1)\sum_{m=-l}^{l} c_{l,m}^2$ follows the spectrum of randomly oriented dipoles of Voorhies et al (2002) for sources at the planet's reference radius r_p.

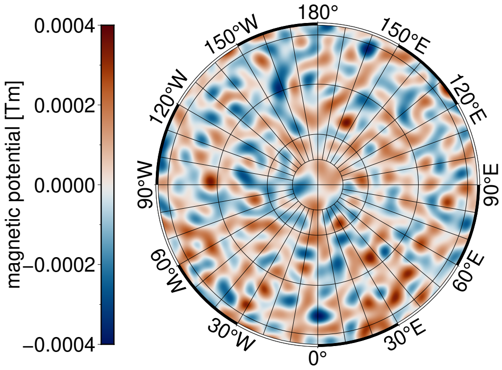

Fig. 5 "True" potential on the planet's surface for spherical harmonic coefficients $\mathbf{c}_{\mathrm{True}}$. The field is shown north of latitude 58° N.

To create data that follow a realistic spacecraft orbit, we used the longitude, latitude, and radial positions of the MESSENGER spacecraft collected between March and April of 2013 with altitude less than 600 km above Mercury's reference radius of 2440 km. The longitudinal and latitudinal data locations cover the region between latitudes 61° N and 84° N (fig. 6a). We lowered the altitude of the data locations by 200 km compared to the spacecraft altitude to allow for resolving the spatial pattern of the potential field of fig. 5. The data radial positions (2440 km + altitude) are lowest close to the north pole and increase in altitude towards latitude 60° N (fig. 6a). To create our test data, we evaluate the spatial derivative of the potential in fig. 5 at these data locations and add Gaussian random noise of magnitude 1% of the root mean square of each component (radial, longitudinal, colatitudinal) to the data, similar to the noise used by Plattner and Johnson (2023).

From these test data, we solved for the regionally representative spherical harmonic coefficients $\bar{\mathbf{c}}$ using the classical Slepian functions (experiment 1) of Simons et al (2006); Simons and Dahlen (2006), the fixed altitude cognizant Slepian functions (experiment 2) of Plattner and Simons (2017) adapted to the radial component only, and the variable altitude cognizant Slepian functions (experiment 3) of section 3.1. For experiment 1, we constructed the classical Slepian functions for the latitudinal band $R = [61° \mathrm{N}, 84° \mathrm{N}]$ following the approach of Simons et al (2006) and Simons and Dahlen (2006). We then evaluated these Slepian functions using eq. (31), but replaced the coefficients $g_{l,m;j}$ with the corresponding Slepian coefficients from the construction of Simons et al (2006) and Simons and Dahlen (2006). The construction of the optimization problem that yields the classical Slepian functions does not depend on

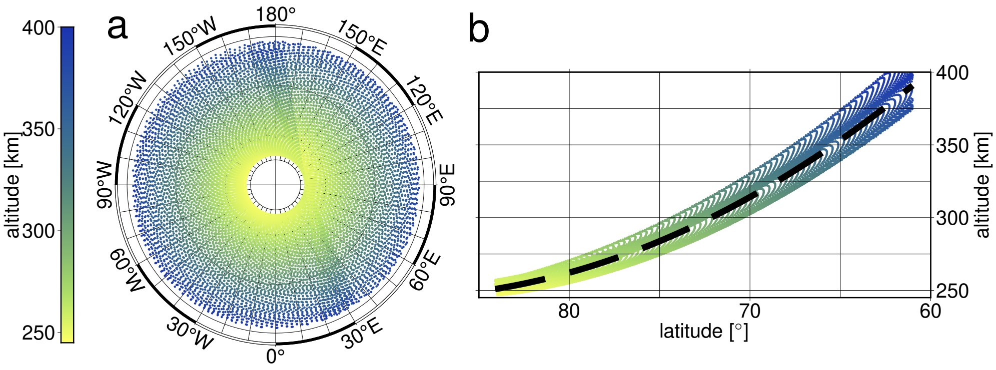

Fig. 6 Data locations used for numerical experiments. Altitude is above a planetary reference radius of $r_p = 2440\,\text{km}$. (a) Polar projection of data locations shown north of latitude 58° N. (b) Latitude versus altitude of data locations. Dashed line indicates the best-fitting polynomial of degree 2 through the cosine of the colatitude.

a radial position, but the functions themselves can be evaluated at individual radial positions (eq. 31). For experiment 2, the fixed altitude cognizant Slepian functions are constructed for the same region R as the classical Slepian functions but for the altitude 300 km above the reference radius $r_p = 2440\,\text{km}$. This corresponds to the average altitude of the data in fig. 6b. For experiment 3, the variable altitude cognizant Slepian functions are constructed for the same region as the classical and fixed altitude cognizant Slepian functions, but the radial position $r = \tilde{r}(\theta, \phi)$ is given by a polynomial of degree 2 that is fitted through the radial positions of the data as a function of the cosine of the colatitude (fig. 6b).

To determine the optimal number J of Slepian functions to use for each of these three experiments, we calculated the relative mean squared error (mse) of the solutions $\bar{\mathbf{c}}$ for a range of values for J, where

$$\text{relative mse} = \frac{|V_{\text{True}} - V_{\text{inv}}|_R}{|V_{\text{True}}|_R} \tag{75}$$

for $V_{\text{True}} = \mathbf{c}_{\text{True}}{}^{\top}\mathcal{Y}$ and $V_{\text{inv}} = \bar{\mathbf{c}}^{\top}\mathcal{Y}$ and the norm $|\cdot|_R$ defined in eq. (3). The best solution (i.e., lowest relative mse) obtained for experiment 1 using the classical Slepian functions had a relative mse of 0.85 for $J = 100$ (fig. 7a). The best solution for experiment 2 using the fixed altitude cognizant Slepian functions achieved a relative mse of 0.41 for $J = 485$ (fig. 7b). For experiment 3, the best solution using the variable altitude cognizant Slepian functions had a relative mse of 0.21 for $J = 500$ (fig. 7c).

The spatial patterns of these three solutions (fig. 8: classical for $J = 100$, fixed for $J = 485$, and variable for $J = 500$) show that the fixed (fig. 8b) as well as the variable (fig. 8c) altitude cognizant Slepian functions reveal the short-scale nature of the true potential (fig. 5), whereas the classical Slepian functions (fig. 8a) lack the short-scale structure. The absolute misfit of the solution using the classical Slepian functions (fig. 8d) is larger throughout the region R compared to the absolute misfit using the fixed (fig. 8e) and variable (fig. 8f) altitude cognizant Slepian functions. The variable

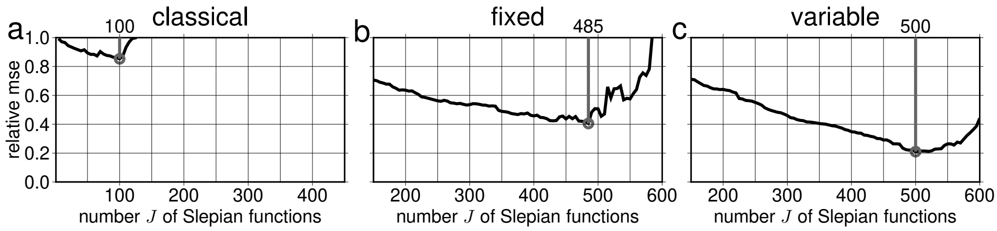

Fig. 7 Relative mean squared error depending on the number J of Slepian functions for (a) classical Slepian functions, (b) fixed altitude cognizant Slepian functions, (c) variable altitude cognizant Slepian functions.

altitude cognizant Slepian functions outperform the fixed altitude cognizant Slepian functions particularly in the region between latitudes 70° N and 84° N (*cf.* fig. 8e to fig. 8f), where the data are available at a lower altitude (fig. 6b). The overall relative mse of the solution using the variable altitude cognizant Slepian functions is half the corresponding relative mse of the solution using the fixed altitude cognizant Slepian functions (0.21 vs 0.41, see fig. 7).

5 Discussion and Conclusions

We present an approach to construct a basis of functions for solving for a regionally-valid potential field on a planet's surface from regionally-available spatial derivative data at spacecraft altitude. An example for such a situation is solving for the magnetic potential from magnetic field measurements, or solving for the gravity potential from acceleration measurements. The difference between the presented approach (variable altitude cognizant Slepian functions) and the basis of functions of Plattner and Simons (2017) (fixed altitude cognizant Slepian functions) is that the variable altitude cognizant functions can take into account a reference spacecraft altitude that varies with longitude and latitude. We show an example, where the variable altitude cognizant Slepian functions produce a result with a substantially lower misfit compared to the fixed altitude cognizant Slepian functions. This new approach is most beneficial compared to fixed altitude cognizant Slepian functions when the best fitting surface through the spacecraft radial positions correlates with longitude and/or latitude. For spacecraft radial positions that, on average, lie on a sphere, the variable altitude cognizant Slepian functions default to the fixed altitude cognizant Slepian functions. The variable and fixed altitude cognizant Slepian functions outperform the classical Slepian functions for the task of solving for a potential on the surface of a planet from data at spacecraft altitude because both types of altitude cognizant Slepian functions take into account the downward continuation from a reference spacecraft altitude, which the classical Slepian functions do not.

Instead of using the local (variable) altitude cognizant Slepian functions, one could calculate a potential field directly by solving eq. (39) or eq. (69) using a singular value approach. The advantage of using altitude cognizant Slepian functions over such an approach is that a single construction of altitude cognizant Slepian functions can be

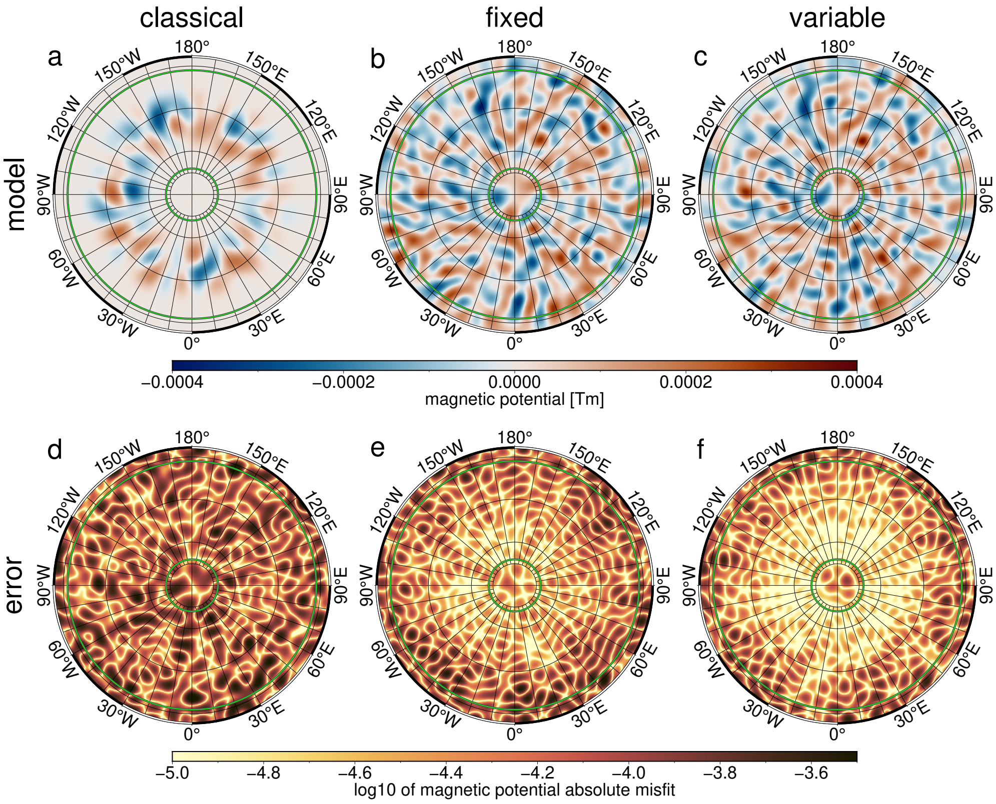

Fig. 8 Inversion results using (a) classical, (b) fixed, and (c) variable altitude cognizant Slepian functions, and their error compared to the known model (fig. 5) for (d) classical, (e) fixed, and (f) variable altitude cognizant Slepian functions. Green circles indicate the boundary of the region R.

used to solve for a potential field from randomly subsampled data. This makes bootstrapping (see Plattner and Johnson, 2023) computationally efficient. For symmetric regions R such as spherical caps or rings, the computation of (altitude cognizant) Slepian functions is particularly numerically efficient, see, e.g., Plattner and Simons (2014).

In the presented numerical examples (fig. 7), the relative mse was calculated using the known true potential. In real applications, the true potential is not known. In such a situation, the relative mse can be estimated using a bootstrapping approach, in which a fraction of the data are used to solve for the potential, and the remaining data are used to calculate the mse, see Plattner and Johnson (2023).

Acknowledgments. AMP acknowledges support from NASA's Planetary Science Early Career Award Program (grant number 80NSSC20K1080). We thank the editor Frederik J. Simons and reviewer Timothée Delcourt for their helpful comments. All figures were created using the Generic Mapping Tools, Version 6 (Wessel et al, 2019). Software to reproduce the results of this paper are available from https://zenodo.

org/doi/10.5281/zenodo.13737507 and require the Slepian software package available from https://zenodo.org/doi/10.5281/zenodo.598177 with installation instructions on https://github.com/Slepian/Slepian.

References

Albertella A, Sacerdote F (2001) Using Slepian functions for local geodetic computations. Boll Geod Sci Affini 60(1):1–14

Alken P, Thébault E, Beggan CD, et al (2021) International geomagnetic reference field: the thirteenth generation. Earth Planets Space 73(49). https://doi.org/10.1186/s40623-020-01288-x

Bates A, Khalid Z, Kennedy R (2017) Efficient computation of Slepian functions for arbitrary regions on the sphere. IEEE Trans Signal Process 65(16):4379–4393. https://doi.org/10.1109/TSP.2017.2712122

Benkhoff J, van Casteren J, Hayakawa H, et al (2010) BepiColombo — Comprehensive exploration of Mercury: Mission overview and science goals. Planet Space Sci 58:2–20. https://doi.org/10.1016/j.pss.2009.09.020

Blakely RJ (1995) Potential Theory in Gravity & Magnetic Applications. Cambridge University Press

Chambodut A, Panet I, Mandea M, et al (2005) Wavelet frames: An alternative to spherical harmonic representation of potential fields. Geophys J Int 163(3):875–899. https://doi.org/10.1111/j.1365-246X.2005.02754.x

Eshagh M (2009) Spatially restricted integrals in gradiometric boundary value problems. Artif Satell 44(4):131–148. https://doi.org/10.2478/v10018-009-0025-4

Farquharson CG, Oldenburg DW (1998) Non-linear inversion using general measures of data misfit and model structure. Geophys J Int 134:213–227. https://doi.org/10.1046/j.1365-246x.1998.00555.x

Finlay CC, Kloss C, Olsen N, et al (2020) The CHAOS-7 geomagnetic field model and observed changes in the South Atlantic Anomaly. Earth Planets Space 72(156). https://doi.org/10.1186/s40623-020-01252-9

Freeden W, Gerhards C (2010) Poloidal and toroidal field modeling in terms of locally supported vector wavelets. Math Geosc 42:817–838. https://doi.org/10.1007/s11004-009-9262-0

Freeden W, Schreiner M (2006) Local multiscale modelling of geoid undulations from deflections of the vertical. J Geod 79:641–651. https://doi.org/10.1007/s00190-005-0017-5

Freeden W, Windheuser U (1997) Combined spherical harmonic and wavelet expansion – a future concept in Earth's gravitational determination. Appl Comput Harmon Anal 4:1–37. https://doi.org/10.1006/acha.1996.0192

Genova A, Goossens S, Lemoine FG, et al (2016) Seasonal and static gravity field of Mars from MGS, Mars Odyssey and MRO radio science. Icarus 272:228–245. https://doi.org/10.1016/j.icarus.2016.02.050

Genova A, Goossens S, Mazarico E, et al (2019) Geodetic evidence that Mercury has a solid inner core. Geophys Res Lett 46. https://doi.org/10.1029/2018GL081135

Gerhards C (2012) Locally supported wavelets for the separation of spherical vector fields with respect to their sources. Int J Wavelets Multiresolution Inf Process 10(4). https://doi.org/10.1142/S0219691312500348

Gerhards C (2014) A combination of downward continuation and local approximation for harmonic potentials. Inverse Probl 30(8). https://doi.org/10.1088/0266-5611/30/8/085004

Goossens S, Sabaka TJ, Wieczorek MA, et al (2019) High-resolution gravity field models from GRAIL data and implications for models of the density structure of the Moon's crust. J Geophys Res 125:e2019JE006086. https://doi.org/10.1029/2019JE006086

Grünbaum FA, Longhi L, Perlstadt M (1982) Differential operators commuting with finite convolution integral operators: some non-Abelian examples. SIAM J Appl Math 42(5):941–955. https://doi.org/10.1137/0142067

Holschneider M, Chambodut A, Mandea M (2003) From global to regional analysis of the magnetic field on the sphere using wavelet frames. Phys Earth Planet Inter 135:107–124. https://doi.org/10.1016/S0031-9201(02)00210-8

Hood LL (2015) Initial mapping of Mercury's crustal magnetic field: Relationship to the Caloris impact basin. Geophys Res Lett 42:10565–10572. https://doi.org/10.1002/2015GL066451

Hood LL (2016) Magnetic anomalies concentrated near and within Mercury's impact basins: Early mapping and interpretation. J Geophys Res 121:1016–1025. https://doi.org/10.1002/2016JE005048

Jahn K, Bokor N (2012) Vector Slepian basis functions with optimal energy concentration in high numerical aperture focusing. Optics Comm 285:2028–2038. https://doi.org/10.1016/j.optcom.2011.11.107

Jahn K, Bokor N (2014) Revisiting the concentration problem of vector fields within a spherical cap: A commuting differential operator solution. J Fourier Anal Appl 288(2):421–451. https://doi.org/10.1007/s00041-014-9324-7

Jakosky BM, Lin RP, Grebowsky JM, et al (2015) The Mars Atmosphere and Volatile Evolution (MAVEN) mission. Space Sci Rev 195:3–48. https://doi.org/10.1007/s11214-015-0139-x

Jekeli C (2007) Potential theory and static gravity field of the Earth. In: Schubert G (ed) Treatise on Geophysics, Vol 3, 1st edn. Elsevier, chap 3.02, p 11–42

Kasaba Y, Takashima T, Matsuda S, et al (2020) Mission data processor aboard the BepiColombo Mio spacecraft: Design and scientific operation concept. Space Sci Rev 216(36). https://doi.org/10.1007/s11214-020-00658-x

Landau HJ, Pollak HO (1961) Prolate spheroidal wave functions, Fourier analysis and uncertainty — II. Bell Syst Tech J 40(1):65–84. https://doi.org/10.1002/j.1538-7305.1961.tb03977.x

Langlais B, Houliez ETA, Purucker ME, et al (2019) A new model of the crustal magnetic field of Mars using MGS and MAVEN. J Geophys Res 124:1542–1569. https://doi.org/10.1029/2018JE005854

Lemoine FG, Luthcke SB, Rowlands DD, et al (2007) The use of mascons to resolve time-variable gravity from GRACE. In: Tregoning P, Rizos C (eds) Dynamic Planet. Springer, chap 35, p 231–236

Lemoine FG, Goossens S, Sabaka TJ, et al (2013) High-degree gravity models from GRAIL primary mission data. J Geophys Res 118:1676–1699. https://doi.org/10.1002/jgre.20118

Maniar H, Mitra PP (2005) The concentration problem for vector fields. Int J Bioelectromagn 7(1):142–145

Mayer C, Maier T (2006) Separating inner and outer Earth's magnetic field from CHAMP satellite measurements by means of vector scaling functions and wavelets. Geophys J Int 167(3):1188–1203. https://doi.org/10.1111/j.1365-246X.2006.03199.x

Michel V (2002) Scale continuous, scale discretized, and scale discrete harmonic wavelets for the outer and the inner space of a sphere and their application to an inverse problem in geomathematics. Appl Comput Harmon Anal 12:77–99. https://doi.org/10.1006/acha.2001.0369

Michel V, Simons FJ (2017) A general approach to regularizing inverse problems with regional data using Slepian wavelets. Inverse Probl 33(12). https://doi.org/10.1088/1361-6420/aa9909

Michel V, Plattner AM, Seibert K (2022) A unified approach to scalar, vector, and tensor Slepian functions on the sphere and their construction by a commuting operator. Anal Appl 20(5):947–988. https://doi.org/10.1142/S0219530521500317

Mitra PP, Maniar H (2005) Local basis expansions for MEG source localization. Int J Bioelectromagn 7(2):30–33

Morschhauser A, Lesur V, Grott M (2014) A spherical harmonic model of the lithospheric magnetic field of Mars. J Geophys Res 119:1162–1188. https://doi.org/10.1002/2013JE004555

Oliveira JS, Langlais B, Pais MA, et al (2015) A modified equivalent source dipole method to model partially distributed magnetic field measurements, with application to Mercury. J Geophys Res 120:1075–1094. https://doi.org/10.1002/2014JE004734

Olsen N, Hulot G, Sabaka TJ (2007) The present field. In: Schubert G (ed) Treatise on Geophysics, Vol 5, 1st edn. Elsevier, chap 5.02, p 33–75

Panet I, Chambodut A, Diament M, et al (2006) New insights on intraplate volcanism in French Polynesia from wavelet analysis of GRACE, CHAMP, and sea surface data. J Geophys Res 111:B09403. https://doi.org/10.1029/2005JB004141

Plattner A, Simons FJ (2014) Spatiospectral concentration of vector fields on a sphere. Appl Comput Harmon Anal 36:1–22. https://doi.org/10.1016/j.acha.2012.12.001

Plattner A, Simons FJ (2015a) High-resolution local magnetic field models for the Martian South Pole from Mars Global Surveyor data. J Geophys Res 120:1543–1566. https://doi.org/10.1002/2015JE004869

Plattner A, Simons FJ (2015b) Potential-field estimation using scalar and vector Slepian functions at satellite altitude. In: Freeden W, Nashed MZ, Sonar T (eds) Handbook of Geomathematics, 2nd edn. Springer, Heidelberg, Germany, p 2003–2055, https://doi.org/10.1007/978-3-642-54551-1_64

Plattner A, Simons FJ (2017) Internal and external potential-field estimation from regional vector data at varying satellite altitude. Geophys J Int 211:207–238. https://doi.org/10.1093/gji/ggx244

Plattner AM, Johnson CL (2021) Mercury's Northern Rise core-field magnetic anomaly. J Geophys Res 48:e2021GL094695. https://doi.org/10.1029/2021GL094695

Plattner AM, Johnson CL (2023) Local spherical harmonic power spectra from local magnetic or gravity data. Geophys J Int 236(3):1668–1679. https://doi.org/10.1093/gji/ggad487

Plattner AM, Johnson CL, Styczinski MJ, et al (2023) On Ganymede's magnetic quadrupolar strength. Planet Sci 4(134). https://doi.org/10.3847/PSJ/acde7f

Purucker ME, Nicholas JB (2010) Global spherical harmonic models of the internal magnetic field of the Moon based on sequential and coestimation approaches. J Geophys Res 115:E12007. https://doi.org/10.1029/2010JE003650

Rowlands DD, Luthcke SB, McCarthy JJ, et al (2010) Global mass flux solutions from GRACE: A comparison of parameter estimation strategies — Mass concentrations versus Stokes coefficients. J Geophys Res 115:B01403. https://doi.org/10.1029/2009JB006546

Simons FJ, Dahlen FA (2006) Spherical Slepian functions and the polar gap in geodesy. Geophys J Int 166(3):1039–1061, doi: 10.1111/j.1365–246X.2006.03065.x

Simons FJ, Dahlen FA, Wieczorek MA (2006) Spatiospectral concentration on a sphere. SIAM Rev 48(3):504–536. https://doi.org/10.1137/S0036144504445765

Slepian D, Pollak HO (1961) Prolate spheroidal wave functions, Fourier analysis and uncertainty — I. Bell Syst Tech J 40(1):43–63. https://doi.org/10.1002/j.1538-7305.1961.tb03976.x

Solomon SC, McNutt RLJr., Gold RE, et al (2007) MESSENGER mission overview. Space Sci Rev 131:3–39. https://doi.org/10.1007/s11214-007-9247-6

Thébault E, Mandea M, Schott JJ (2006a) Revised spherical cap harmonic analysis (R-SCHA): Validation and properties. J Geophys Res 111:B01102. https://doi.org/10.1029/2005JB003836

Thébault E, Schott JJ, Mandea M (2006b) Modeling the lithospheric magnetic field over France by means of revised spherical cap harmonic analysis (R-SCHA). J Geophys Res 111:B05102. https://doi.org/10.1029/2005JB004110

Toyoshima M, Shibuya H, Matsushima M, et al (2008) Equivalent source mapping of the lunar crustal magnetic field using ABIC. Earth Planets Space 60:365–373. https://doi.org/10.1186/BF03352801

Tsunakawa H, Takahashi F, Shimizu H, et al (2015) Surface vector mapping of magnetic anomalies over the Moon using Kaguya and Lunar Prospector observations. J Geophys Res 120:1160–1185. https://doi.org/10.1002/2014JE004785

Voorhies CV, Sabaka TJ, Purucker M (2002) On magnetic spectra of Earth and Mars. J Geophys Res 107(E6):5034. https://doi.org/10.1029/2001JE001534

Wessel P, Luis JF, Uieda L, et al (2019) The Generic Mapping Tools version 6. Geochem Geophys Geosys 20:5556–5564. https://doi.org/10.1029/2019GC008515

Wieczorek MA, Simons FJ (2005) Localized spectral analysis on the sphere. Geophys J Int 162(3):655–675. https://doi.org/10.1111/j.1365-246X.2005.02687.x

Wittick PT, Russell RP (2019) Mixed-model gravity representations for small celestial bodies using mascons and spherical harmonics. Celest Mech Dyn Astr 131(31). https://doi.org/10.1007/s10569-019-9904-6